Journal of Inorganic and Organometallic Polymers and Materials
https://doi.org/10.1007/s10904-021-02077-z

A Facile Preparation of Zinc Cobaltite ($ZnCo_2O_4$) Nanostructures for Promising Supercapacitor Applications

M. Silambarasan[1] · P. S. Ramesh[2] · D. Geetha[3] · K. Ravikumar[1] · H. Elhosiny Ali[4,5] · H. Algarni[4] · P. Soundhirarajan[6] · Kamlesh V. Chandekar[7] · Mohd. Shkir[4]

Received: 11 January 2021 / Accepted: 21 July 2021

Abstract

Hybrid nanocomposites have shown their excellent potential in energy storage devices particularly in electrochemical supercapacitors to meet the forthcoming demand in the energy sector applications. Novel hybrid composited displayed the dual nature of electrochemical double layer and pseudocapacitive behaviour, which makes them more advantageous in supercapacitor device fabrication. Zinc cobaltite ($ZnCo_2O_4$) nanostructures have been prepared by precipitation route and the structural, optical and electrochemical properties of the final product were analyzed. X-ray pattern showed the spinal cubic phase structure with fine nano-crystallites. The FTIR and Raman spectrum confirmed the presence of surface functional groups and confirmed the formation of high-quality $ZnCo_2O_4$ nanocrystals. XPS and EDX spectrum showed the high purity and good crystallinity nature of the as-prepared $ZnCo_2O_4$ nanocrystal. FE-SEM and TEM analysis exhibits the bundle like morphology of the final product. Finally, the as-prepared $ZnCo_2O_4$ nanostructure was investigated by cyclic voltammetry (CV), galvanic charge–discharge analysis (GCD) and electrochemical impedance spectroscopy (EIS) to check its suitability. The electrochemical investigation demonstrated the highest capacitance of 159 F g^{-1} at 2 mA cm^{-2} in 2 M KOH electrolyte and the long cyclic test showed the 92% initial capacitance retention over 2500 cycles. It reveals/demonstrated that the spinel $ZnCo_2O_4$ nanostructures own a promising usage in devices for electrochemical energy storage.

Keywords $ZnCo_2O_4$ · Spinel · Supercapacitor · Nanostructures · Co-precipitation

1 Introduction

The shortage in conventional energy source forced worldwide researchers to focus on the alternative source to meet the depletion of natural resources. Another major issue is global warming due to the emission of greenhouse gases from automobile and industries. To overcome these issues in present and also in future, various energy sources have been addressed but they still need development to sort out their issues and then searching for alternative energy is more important nowadays [1–3]. Identification of new and clean energy is part of the problem and the other side is storing the as-produced energy in the device for future usage [4, 5]. Though the batteries are capable of providing the required energy due to their low power density and they couldn't be used in all electrical devices [6]. These problems were overcome in electrochemical supercapacitor (ESc) by the factor of 10–100 times than the batteries.

Electrochemical supercapacitors (ESc) are recently attracted worldwide researchers' interest owing to their

✉ M. Silambarasan
silambanphy@gmail.com

1 Vivekanandha College of Arts and Sciences for Women (Autonomous), Tiruchengode, Tamil Nadu 637205, India

2 Department of Physics, Thiru Kolanjiappar Government Arts College, Viruthachalam, Tamil Nadu 606001, India

3 Department of Physics, Annamalai University, Annamalai Nagar, Chidambaram, Tamil Nadu 608002, India

4 Department of Physics, College of Science, King Khalid University, Abha 61413, Saudi Arabia

5 Physics Department, Faculty of Science, Zagazig University, Zagazig 44519, Egypt

6 Department of Physics, St. Joseph University, Dimapur, Nagaland 797115, India

7 Department of Physics, Rayat Shikshan Sanstha's, Karmaveer Bhaurao Patil College, Vashi, Navi Mumbai 400703, India

increase in demand for high power density and reliable energy deliverable applications for military, electronics, automobile, space, etc. [7–9]. Supercapacitors have peculiar properties like higher power density, fast charge/discharge rate, exceptional cycle life and safety [10, 11]. In recent years, significant progress has been equipped in the supercapacitor devices; however, the proposed electrode materials exhibited a low energy density and limited by their poor cyclic stability and rate performance [12, 13]. In general, electroactive materials have a major influence on the supercapacitor performance in terms of power–energy density, capacity rate of self-discharge and cycling stability. To overcome these inadequacies of supercapacitor performance, various electroactive materials have been used such as activated carbon [14, 15] conductive polymer [13, 16] and metal oxides [17, 18]. Though there was much hybrid metal oxide nanocomposite existing [19–25] for many application like photocatalyst, hydrogen storage [26–36] with remarkable characteristics, still serious issues like poor cycle & action rate were associated with them. Hence the development of ideal electrode material is still a challenge. Based on the charge storing nature, supercapacitors are mainly divided into electrical double-layer capacitors (EDLCs) and fast, reversible faradic pseudo-capacitors, respectively [2, 3].

Recently AB_2O_4 based spinel structure binary metal oxide has been intensively investigated as potentially active electrode material for supercapacitors owing to their ideal stoichiometric spinel structure with several oxidation states [37, 38]. In which, zinc cobaltite ($ZnCo_2O_4$) is a usual spinel structure, where zinc ions and trivalent Co ions are occupied one-eighth of tetrahedral (A) and one-half of octahedral (B) sites, respectively [39]. Interestingly, zinc cobaltite nanostructured material has been widely used in gas sensor [40], Li-ion batteries [41] and electro-catalyst application [42] due to their exceptional characteristics of electronic structure. The morphology, microstructure, particle size, surface interface and stoichiometry of $ZnCo_2O_4$ material play an essential role in the electrochemical performances. $ZnCo_2O_4$ nanomaterials with different morphologies have been rationally synthesized such as nanowires [43], nanorods [44], nanotubes [45], and nanosheets [46], and the capacitors based on them have shown greatly enhanced electrochemical performances.

Xu et al. [47] have prepared controlled morphology of $ZnCo_2O_4$ through the facile process and obtained nanowires. The electrochemical analysis of $ZnCo_2O_4$ showed the highest capacitance of 776.2 F g^{-1} with 84.3% of initial capacitance retention. Zhou et al. [45] prepared 1D porous nature of $ZnCo_2O_4$ nanotubes by electrospinning and calculation method. The maximum capacitance of 770 F g^{-1} was achieved and 84% of capacitance retention after 3000 cycles. Hierarchical $ZnCo_2O_4$/nickel foam architectures were prepared by Liu et al. [48] and demonstrated the highest capacitance of 1400 F g^{-1} and 72.5% of capacity retention after 1000 cycles. $ZnCo_2O_4$ (ZC-UAH) composite was prepared by Kumar et al. [49] through hydrothermal technique and ZC-UAH active electrode showed the maximum capacitance of 462.5 C F g^{-1}. Hexagonal-like $ZnCo_2O_4$ nanostructure was prepared by Venkatachalam et al. [50] by hydrothermal method and electrochemical performance of as-prepared electrode material showed the highest capacitance of 845.7 F g^{-1} with 95.3% of cyclic stability. Shang et al. [51] synthesized the $ZnCo_2O_4$ with hollow microspheres by solvothermal method and as-prepared electrode material showed a high surface area of 24.7 m^2 $g^{-1.}$ Mary and Bose [52] prepared the $ZnCo_2O_4$ material with various surfactants to control the morphology of electrode materials and obtained the maximum capacitance of 290.5 F g^{-1}.

Furthermore, a novel chemical precipitation method has been employed for the preparation of mesoporous Zn_2GeO_4 NPs in presence of acacen as a capping agent and $GeCl_4$ as a Ge precursor for the first time. The prepared Zn_2GeO_4/graphene nanocomposites have higher electrochemical hydrogen storage capacity than Zn_2GeO_4 NPs [53]. Salehabadi et al. [54] synthesized a composite of MWCNT loaded with binary metal oxides ($Dy_3Fe_5O_{12}$) acidic propylene glycol through combustion method and it can be used for improving the hydrogen sorbent substrate in electrochemical hydrogen storage devices.

Mortazavi-Derazkola et al. [55] reported the higher photocatalytic activity of Fe_3O_4@SiO_2@TiO_2@Ho NPs than Fe_3O_4@SiO_2@TiO_2 during the degradation of RhB and MO, even after 7 and 6 cycles respectively. The $Nd_2Zr_2O_7$–Nd_2O_3 nanocomposites were prepared by facile and cost-effective method using salicylic acid as new complexing agent and propylene glycol as novel cross-linking agent. This composite demonstrates the novel photocatalyst activity with better performance under UV than Nd_2O_3 sample [56]. Beshkar et al. [57] synthesized a superhydrophobic magnetic polyurethane sponge by immersing a polyurethane sponge in a colloidal suspension of straw soot and magnetic nanoparticles. Ansari et al. [58] prepared the nanocomposites of Fe_2O_3/$CuFe_2O_4$/chitosan through sol–gel auto combustion route. Ansari et al. [59] prepared the $CoTiO_3$/$CoFe_2O_4$ nanocomposite through new sol–gel auto-combustion technique. Ahmadian-Fard-Fini et al. [60] synthesized the carbon dots (CDs) by grape fruit, lemon, turmeric extracts and magnetite NPs were prepared using these bio-compatible capping agents. Consequently, magnetite–carbon dots composite were synthesized as PL sensor for detecting of *Escherichia coli* bacteria. Tavakoli et al. [61] prepared the improved Hummer method to oxidize graphite for the synthesis of graphene oxide (GO) and then it reduced to graphene nanosheets by reduced by pomegranate juice. Salavati-Niasari et al. [62] synthesized the oleylamine capped copper nanocrystals using thermal reduction method.

In these methods, complex methodology and the high-temperature process was adopted to synthesis the various surface morphology of $ZnCo_2O_4$. The rational synthesis of $ZnCo_2O_4$ with controlled morphologies is essential, which can enhance the electrochemical performance. Although owing to its importance, significant research efforts are still needed to further improve the practical use of $ZnCo_2O_4$ in supercapacitor devices. Consequently, it is still a big task to develop a facile and low-temperature methodology to attain spinel $ZnCo_2O_4$ nanostructures, and this has been tried in the current article. In this work, we tried a simplistic approach to attain zinc cobaltite ($ZnCo_2O_4$) nanostructures (NSs) using oxalic acid as precipitant through a simple synthetic process. The $ZnCo_2O_4$ nano-bundle like morphology was achieved by a one-step co-precipitation method with oxalic acid precipitant. The obtained uniform bundle like morphology was used to study the electrochemical behavior. The use of oxalic acid (as a chelating agent) as a precipitant has been well discussed in the literature [63, 64] and no literature documented the synthesis of $ZnCo_2O_4$ using oxalic acid. The prepared material has been characterized by XRD, Raman, FT-IR, XPS, TEM and their electrochemical behavior was explored towards the supercapacitor application.

2 Experimental Details

2.1 Materials and Methods

To synthesis spinel $ZnCo_2O_4$ nanostructures, the following analytical reagents were used for the synthesis of present samples. $Zn(NO_3)_2·6H_2O$, 99% (Alfa Aesar), $Co(NO_3)_2·6H_2O$, 99% (Alfa Aesar), oxalic acid ($H_2C_2O_4·2H_2O$) and double distilled water.

2.2 Preparation

$Zn(NO_3)_2·6H_2O$, $Co(NO_3)_2·6H_2O$ and $H_2C_2O_4·2H_2O$ (oxalic acid) were used as a precursors for the preparation of $ZnCo_2O_4$ via the co-precipitation route. The quantitative amount of $Zn(NO_3)_2·6H_2O$ (2 M) and $Co(NO_3)_2·6H_2O$ (1 M) were dissolved individually in distilled H_2O and $H_2C_2O_4·2H_2O$ was added into it dropwise as precipitant agent with regular stirring. After 30 min of stirring, the resulted suspension was placed in a conical flask and stirred in an oil bath at 90 °C for an additional 5 h. After that, the obtained precipitate was filtered and washed with ethanol and acetone repeatedly. The precipitate was finally dried in a vacuum oven at 80 °C for 6 h and the final product was calcinated at 400 °C for 4 h. A detailed flow chart has been displayed in Fig. 1.

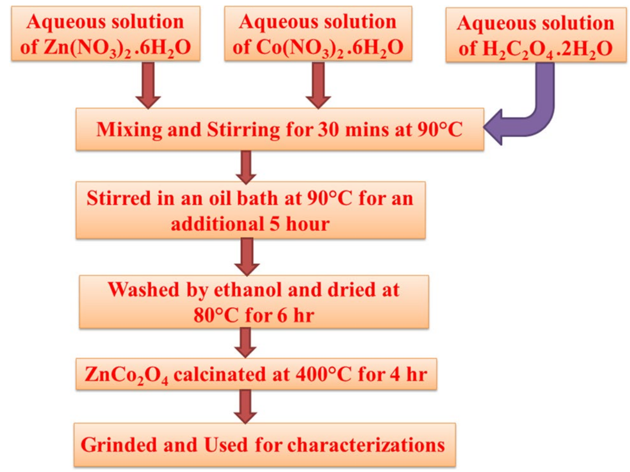

Fig. 1 A simple flow chart to present the experimental procedure

2.3 Characterization and Electrode Preparation Techniques

The phase purity and structure of the prepared sample were analyzed with X-ray powder diffraction (XRD) technique using Cu Kα radiation (D8 ADVANCE from Bruker). The vibration modes inspection of prepared nanomaterials was analyzed with Fourier transform infrared spectra recorded with a spectrometer from Perkin Elmer. A Renishaw Raman microscope having 514.3 nm laser was employed to attain Raman spectra. The elemental composition was analyzed by XPS from Krato Analytical. For morphological/compositional studies, a SUPRA 55, along with EDS instruments and transmission electron microscope (TEM CM-200) were utilized for SAED and HRTEM. The bandgap of $ZnCo_2O_4$ NPs was estimated from the UV–Vis absorption profile recorded with UV-2550 from Shimadzu. The nature towards electrochemical of the prepared NSs a CHI 660C workstation and CV, GCD and EIS tests between 1 and 10 mV were conducted through 3 electrode configuration in a solution of 2 M KOH electrolyte at 300 K. For preparing the electrode from the synthesized NSs of $ZnCo_2O_4$ the earlier reported process has been employed.

3 Results and Discussion

3.1 Structural Analysis

The XRD pattern of the $ZnCo_2O_4$ NSs was shown in Fig. 2a. The characteristic diffraction peaks of (111), (220), (311), (222), (400), (422), (511), (440), (620) and (533) are well indexed to the cubic spinel $ZnCo_2O_4$ nanostructure (JCPDS # 23-1390). The crystallographic structure of the spinel cobaltite was shown in Fig. 2b, which demonstrated that Zn

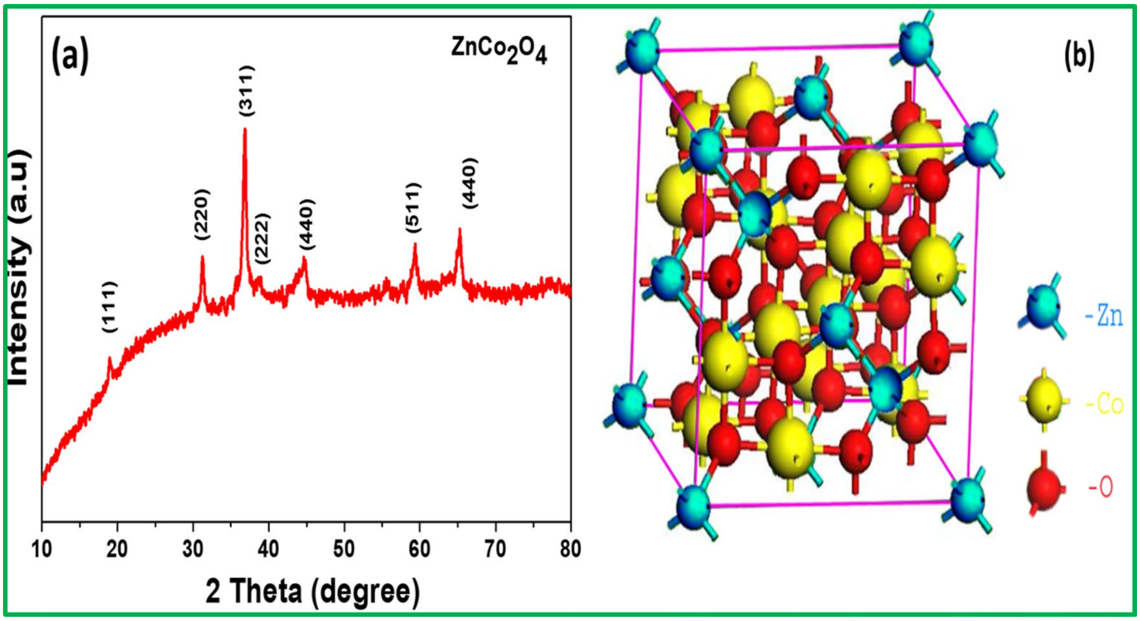

Fig. 2 **a** XRD patterns of spinel $ZnCo_2O_4$ nanostructures prepared by oxalic acid as precipitant and **b** the crystallographic structure of the spinel cobaltite

occupied at the octahedral (B) sites and Co takes place in both tetrahedral (A) and octahedral (B) sites. The crystallite size of the prepared nanocrystals was calculated from the diffraction peak (311) by Scherrer formula $D = 0.94\lambda/\beta\cos\theta$. Based on the high intensity of the diffraction peak, the crystalline size of $ZnCo_2O_4$ nanocrystals was estimated to be 12 nm. Moreover, the absence of additional peaks confirms the high purity of the nanoparticles of $ZnCo_2O_4$.

The FTIR spectrum was employed to get the info about surface functional groups of $ZnCo_2O_4$ nanostructures in the range of 400 to 4000 cm^{-1} and showed in Fig. 3a. The strong and sharp peak was identified at 572 and 668 cm^{-1} are assigned to characteristic peaks of Co–O and Zn–O in the

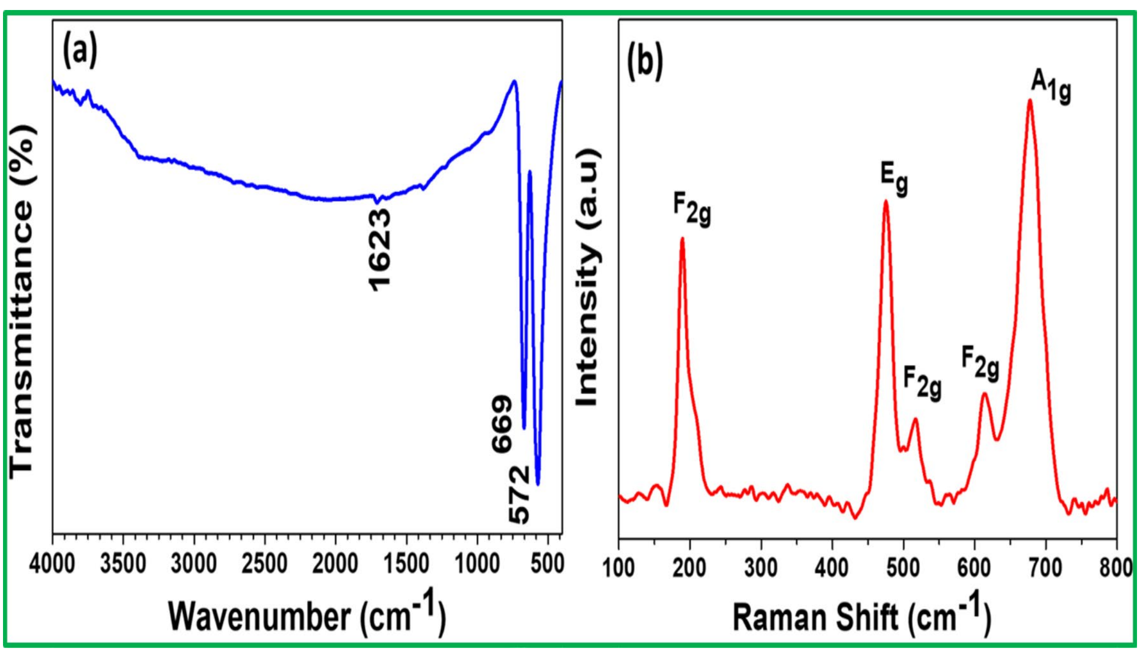

Fig. 3 **a** FTIR and **b** Raman spectrum of the spinel $ZnCo_2O_4$ NSs

prepared samples [65, 66]. The Raman profile of zinc cobaltite NSs was shown in Fig. 3b. Five fundamental Raman modes were observed, which resembles F_{2g} (188.3 cm^{-1}), E_g (476.6 cm^{-1}), F_{2g} (516.4 cm^{-1}), F_{2g} (614.4 cm^{-1}) and A_{1g} (680.8 cm^{-1}) of $ZnCo_2O_4$ phase [42, 67]. Further Raman spectroscopy analysis confirmed the formation of high-quality $ZnCo_2O_4$ NSs. To identify the composition of $ZnCo_2O_4$ nanostructures along with oxidation states, the XPS study was performed and shown in Fig. 4a. In the spectrum (Fig. 4a), the characteristic peaks of Zn 2p, Co 2p, O 1s and C 1s elements are contained in $ZnCo_2O_4$ nanostructures. The appearance of C was due to the air exposure of material electrodes. Figure 4b represents the high-resolution Zn 2p spectrum. The Zn $2p_{1/2}$ and Zn $2p_{3/2}$ main peaks were observed at 1043.4 and 1020.3 eV, respectively. The Co 2p spectrum (Fig. 4c) of the prepared nanocrystals showed the presence of 2 peaks associated to Co $2p_{1/2}$ (BE = 795.2 eV) and Co $2p_{3/2}$ (BE = 780.5 eV) of $ZnCo_2O_4$ phase. The O 1s spectrum in Fig. 4d displayed two peaks at 530.2 and 531.9 eV, which related to metal–oxygen states of spinel $ZnCo_2O_4$ and all peaks of the prepared sample are in good agreement with previously reported works of literature [68]. The XPS result is consistent with XRD and EDAS analysis as mentioned above.

3.2 FESEM/EDAX and TEM Analysis

The morphology of electrode materials and their composition reveals excellent potential in electrochemical performance and hence FESEM combined with EDAX analysis was requested. Figure 5a–c shows FE-SEM images of $ZnCo_2O_4$ nanostructures. A bundle like structures were observed for oxalic acid treated $ZnCo_2O_4$ particles with a diameter of nearly 80–120 nm. The presence of Zn and Co in $ZnCo_2O_4$ nanostructure was studied by EDAX analysis along with composition of elements and shown in Fig. 5d. This spectrum confirmed the presence of Zn, Co and O and the formation of $ZnCo_2O_4$ spinel structure.

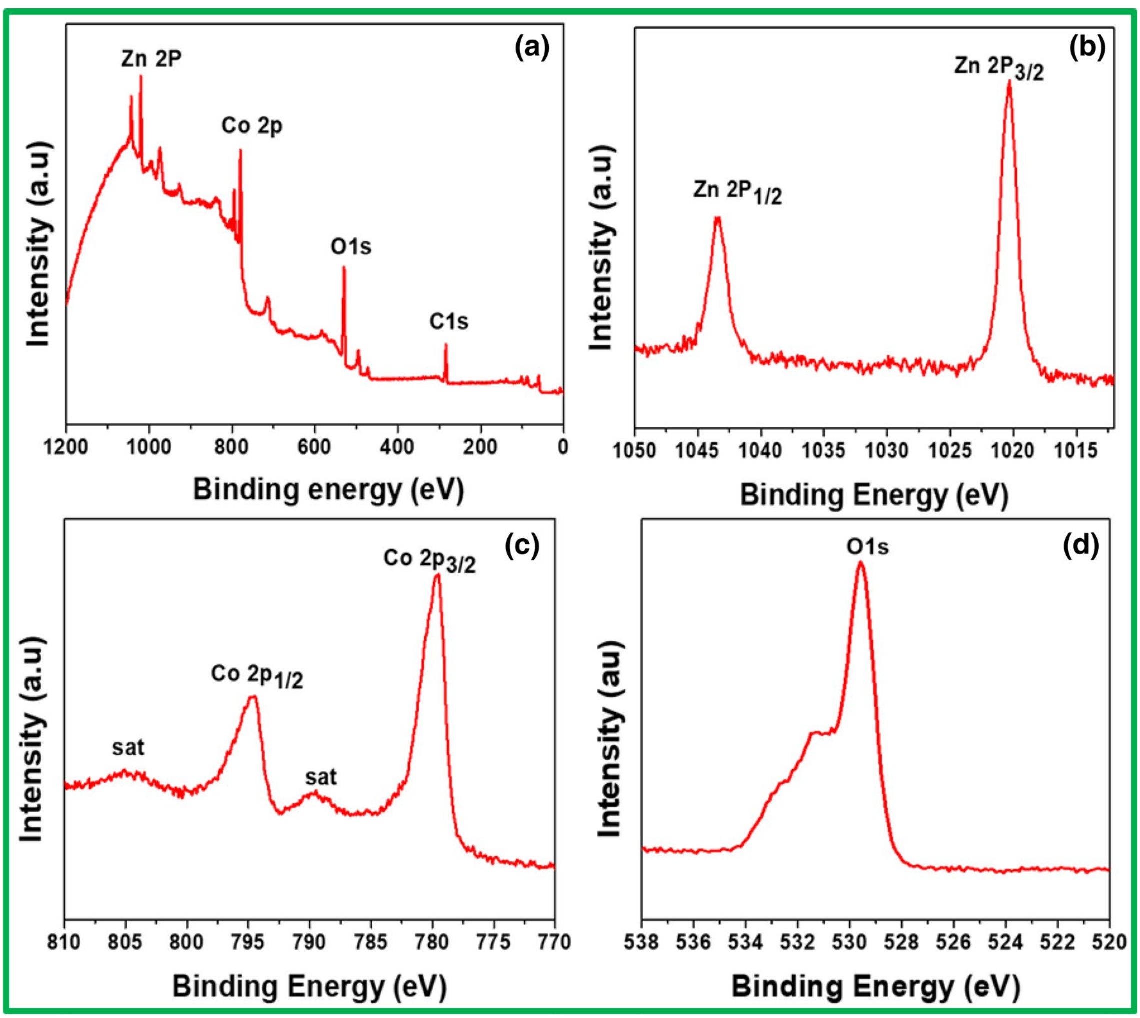

Fig. 4 XPS spectrum of $ZnCo_2O_4$ using oxalic acid **a** full spectrum, **b** Zn 2p, **c** Co 2p and **d** O 1s

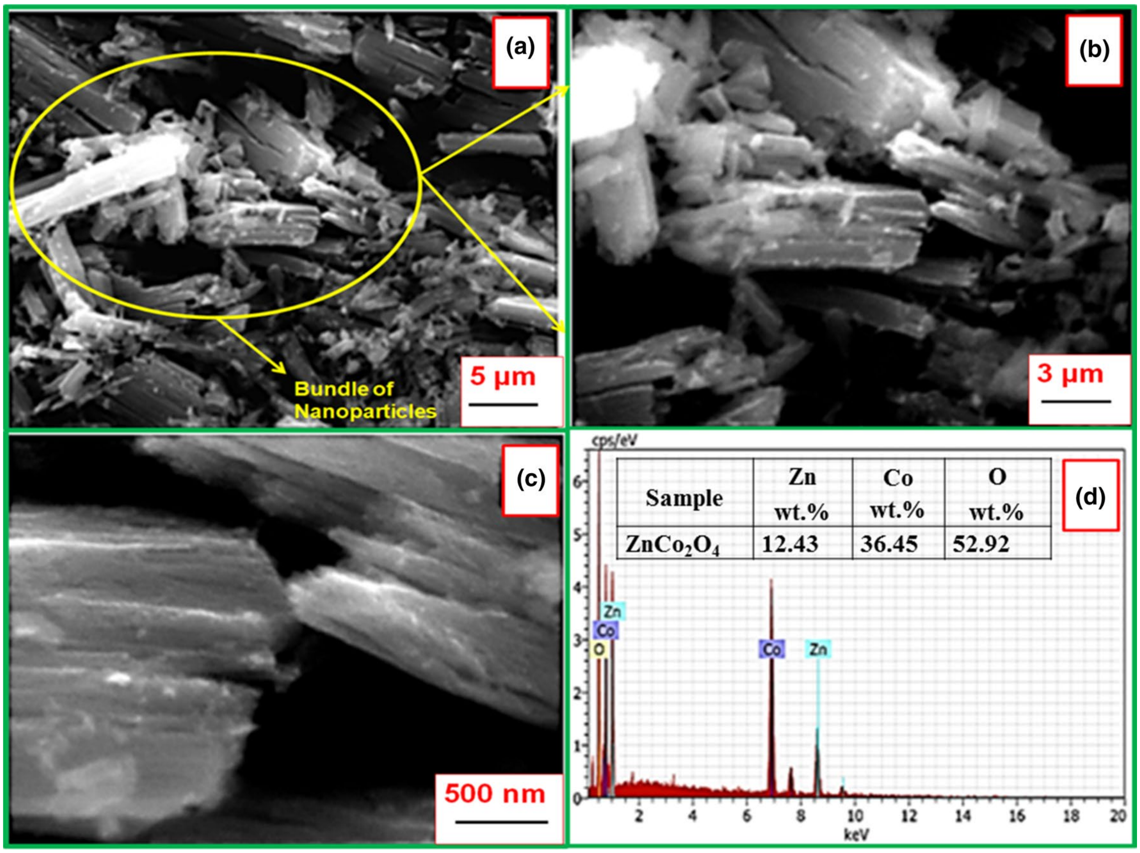

Fig. 5 **a**–**c** FESEM and **d** EDX image of synthesized $ZnCo_2O_4$ nanostructures by oxalic acid as precipitant

The as-prepared sample was further analyzed by TEM/SAED to get clear information on morphology. Figure 6a–c showed the TEM images of the $ZnCo_2O_4$ nanostructures with different magnifications. The bundle like nanoparticle structure was observed and good in agreement with FESEM observations. The nanoparticle bundles have a mean length of ~ 537.6 nm. The pattern in Fig. 6d shows a set of concentric circles and well-defined diffraction rings, which suggests the polycrystalline nature of the $ZnCo_2O_4$ nanoparticles. It was well known that size, shape and homogeneity of the particles depend on the calcination temperature and molar ratio of the precursors [69, 70]. The calcination temperature increases the crystallinity of the nanoparticles. At calcination temperature, continuous agglomerations of fine particles results in rapid growth.

3.3 Absorption Studies (UV–Vis Spectroscopy)

The absorption nature of the $ZnCo_2O_4$ sample was examined by UV–Vis spectroscopy as shown in Fig. 7a. The spectrum showed that the zinc cobaltite has an optical absorption in the region of 265 nm. Figure 7b showed the Tauc plot $[(\alpha h\nu)^2$ vs. $h\nu]$ for the $ZnCo_2O_4$. The bandgap of the bundle like $ZnCo_2O_4$ nanostructure was calculated as 3.8 eV. This bandgap value was higher than the previous reports and in correlation with the earlier reported value by Mariappan et al. [71].

3.4 Electrochemical Analysis

To systematically investigate the electrochemical capacitive properties of the zinc cobaltite nanostructures, CV, GCD, cyclic stability, and electrochemical impedance were tested in 2 M KOH. Electrochemical process of zinc cobaltite

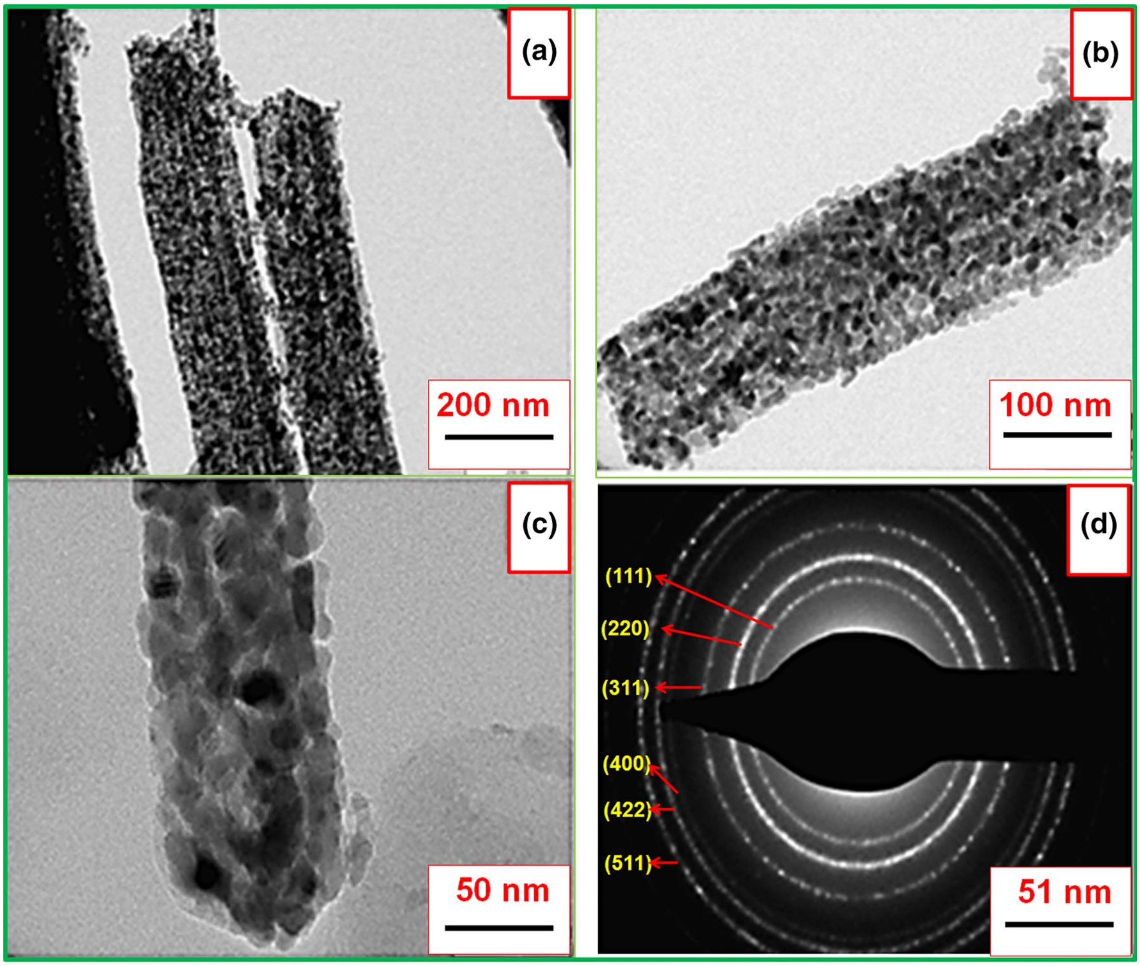

Fig. 6 **a**–**c** TEM and **d** SAED image of $ZnCo_2O_4$ nanostructures

nanostructures is displayed in Fig. 8. Figure 9a reveals representative CV profiles measured at various scanning rate over 1 to 20 mV s^{-1} in − 0.1 to 0.4 V potential regions. From the CV plot, it was perceptible that the oxidation and reduction peak reveals faradaic non-capacitive/battery-like performance of modified zinc cobaltite electrodes by diffusion process [72]. The pair of redox peaks can be observed, which mainly originate from reversible faradaic redox processes on Co^{2+}/Co^{3+} transition linked to OH anions [73]. Moreover, when increasing the scan rate from 5 to 50 mV s^{-1}, the anodic peak gradually moved to positive and the cathodic peak moves to a negative potential. The observation of linear augmentation of the current of oxidation peak exhibits redox progression with controlled diffusion on the surface of the electrode.

To determine supercapacitor performance of prepared electrode, which/the active material is further carefully tested with the help of a GCD method at the current density from 2 to 10 A g^{-1} and plots are revealed in Fig. 9b. From the GCD plots, we can see that the obvious voltage drop was increased with an increase in the current density caused by the internal resisting nature of electrode material. The modified zinc cobaltite electrode envisages non-linear charge/discharge curves, characteristic of non-capacitive faradaic behaviour or battery like behaviour, reliable with

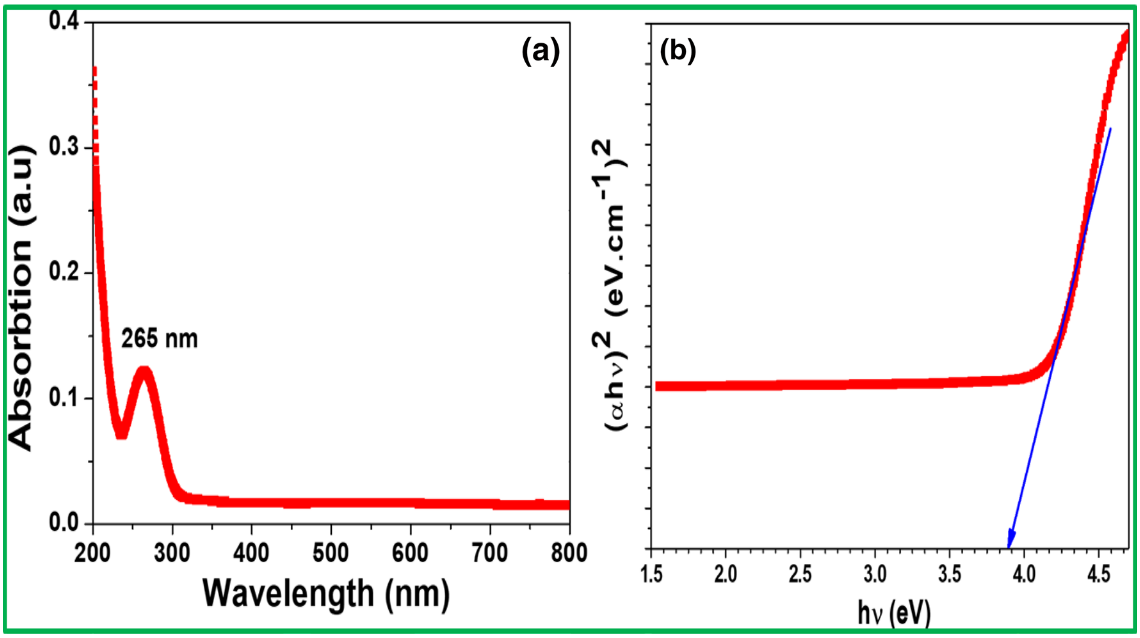

Fig. 7 **a** and **b** UV–Vis spectra and plot of the $(\alpha h\nu)^2$ versus photon energy ($h\nu$) of the $ZnCo_2O_4$ nanocrystals

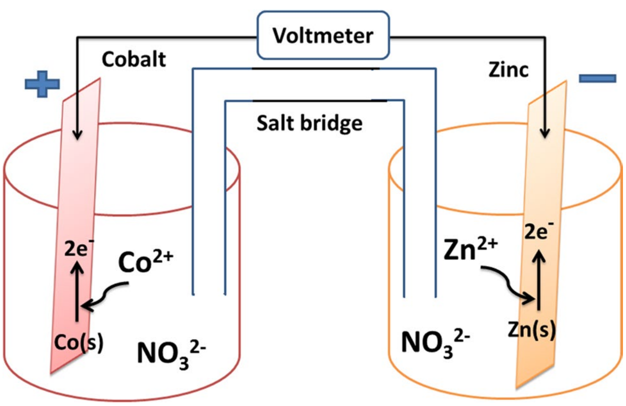

Fig. 8 Electrochemical process of zinc cobaltite nanostructures

CV outcomes. The specific capacitance (C_S, F g^{-1}) values are obtained by the relation:

$$C_S = \frac{I\Delta t}{m\Delta V}.$$

The C_S values of modified $ZnCo_2O_4$ electrode are noticed to be 159, 138, 117, 88, 65 and 42 F g^{-1} for 2, 3, 4, 5, 7.5 and 10 mA cm^{-2} specific current, correspondingly. The quantified supreme C_S is 159 F g^{-1} at 2 mA cm^{-2} and decreased to 42 F g^{-1} at 10 mA cm^{-2} because at a higher density of the current, the rising (IR) voltage fall and inadequate active solid used in redox rejoinder. The synthesis route, specific capacitance, rate property, cyclic stability and electrolyte of the reported articles related to $ZnCo_2O_4$ are tabulated in Table 1, that make impressive comparison of the current and past reported outcomes [39, 46, 74–96].

On the discharge curves, there is no IR drop at high current densities (5 to 10 mA cm^{-2}) and a very small IR drop at low current densities (2 to 3 mA cm^{-2}). This observation indicates that the electrodes have a low internal resistance, which is consistent with the voltammetry results. At a lower current density, the higher capacitance is due to the ample time accessibility of the electrode–electrolyte interface. Also, the evaluation of cycling life tests was performed through repetitive C/D study at a current discharge density of 5 mA cm^{-2}/2500 cycles, as depicted in Fig. 9c. The prepared zinc cobaltite showed excellent cyclic stability and

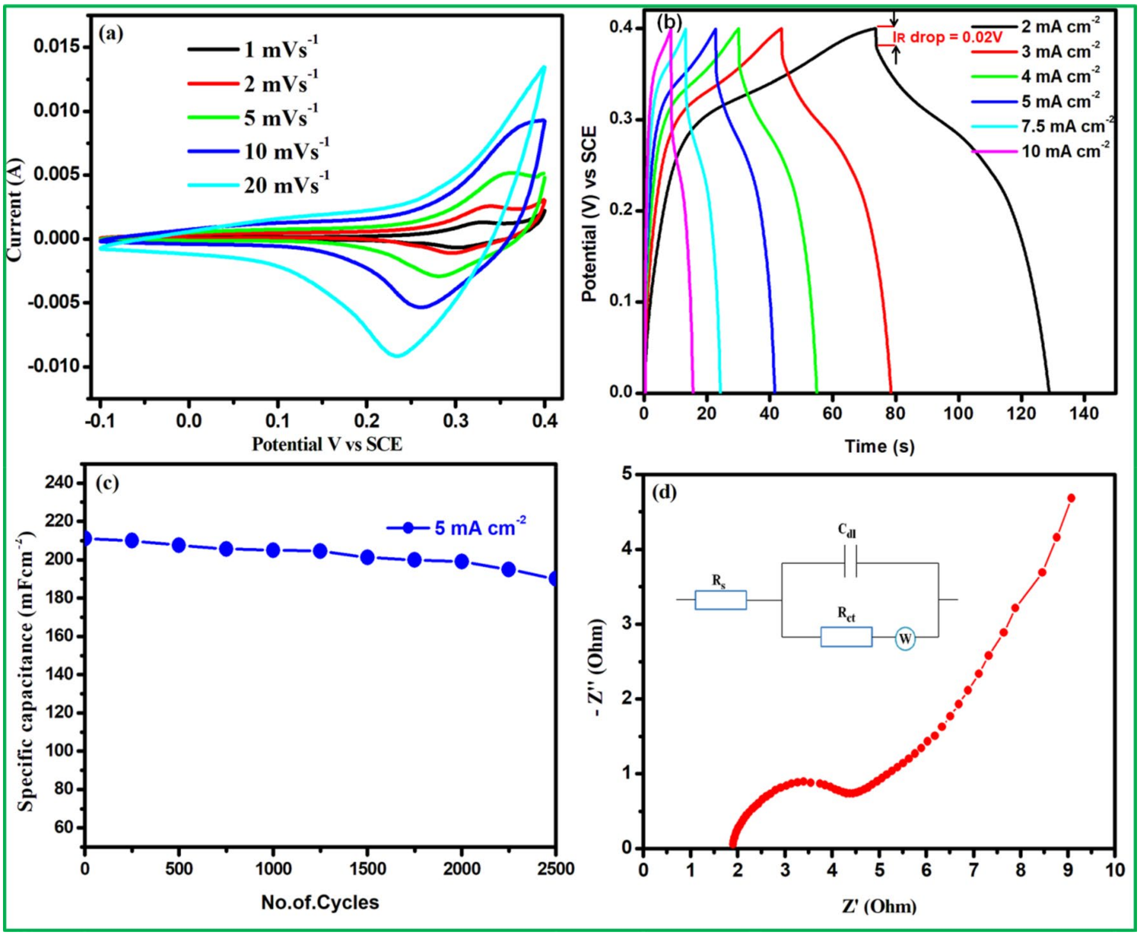

Fig. 9 **a** CV curves of modified $ZnCo_2O_4$ at different scan rates, **b** galvanostatic charge/discharge plots of modified $ZnCo_2O_4$ electrode at different current densities, **c** cyclic stability of the electrode at a constant current of 5 mA cm^{-2} and **d** Nyquist plot $ZnCo_2O_4$ electrode

the capacitance maintained 92% after 2500 cycles. From the obtained results it can be concluded that the proposed spinel $ZnCo_2O_4$ could be a promising electrode for the next generation of energy storage devices.

The EIS was made to inveterate the superlative device resistance after 2500 cycles. Figure 9d presents the outcomes of impedance spectroscopy on the modified $ZnCo_2O_4$ electrodes in 2 M KOH electrolyte solution over 0.1 to 100 kHz ac frequencies. The EIS possess arcs as semicircle over higher to the medium region of frequency and traditional lines at the lower range of frequencies. EIS can be explained using a correspondent circuit displayed in the inset of Fig. 9d, where R_s and R_{ct} are the resistance of solution and charge transfer, correspondingly. The semicircle observed in the high-frequency region from a Nyquist plot gives R_{ct} at electrode/liquid electrolyte interface. The spinel $ZnCo_2O_4$ nanoparticle revealed a solution resistance of 1.8 Ω and a charge transfer resistance of 2.7 Ω. A bundle like $ZnCo_2O_4$ nanoparticles could shorten the ion transport pathway and reduce resistance. The vertical slope observed at lower frequencies corresponds to Warburg impedance (W), suggesting more efficient electrolyte ions and diffusion of

Table 1 Comparison of electrochemical performances of $ZnCo_2O_4$ with previously reported supercapacitors

Sr	Properties Electro-active materials	Synthesis route	Specific capacity (C g^{-1}) or specific capacitance (F g^{-1})	Rate property	Cyclic stability	Electrolyte	References
1	Porous $ZnCo_2O_4$ nanostructures with hexamethylenetetramine (HMT)	Facile hydrothermal route	776.2 F g^{-1} at a current density of 1 A g^{-1}	84.3% Capacity retention at 3 A g^{-1}	–	2 M KOH aqueous solution	[47]
2	One-dimensional (1D) $ZnCo_2O_4$ porous nanotubes (PNTs)	Electro-spinning	770 F g^{-1} at a current density of 10 A g^{-1}	84% Capacity retention at 60 A g^{-1}	89.5% After 3000 cycles at 10 A g^{-1}	6 M KOH aqueous solution	[45]
3	Hierarchical $ZnCo_2O_4$/nickel foam	Polyol refluxing process	~1400 F g^{-1} at a current density of 1 A g^{-1}	72.5% Capacity retention at 20 A g^{-1}	97% After 1000 cycles at 6 A g^{-1}	1 M KOH aqueous solution	[48]
4	$ZnCo_2O_4$ (ZC–urea/ammonium fluoride/hexamethylenetetramine (ZC–UAH) composite	Hydrothermal technique	462.5 C g^{-1} at a current density of 1 A g^{-1} or 1250 F g^{-1} at a current density of 1 A g^{-1}		97.4% After 5000 cycles	2 M KOH aqueous solution	[49]
5	Double hydroxide hexagonal-like $ZnCo_2O_4$ nanostructured	Facile hydrothermal method	845.7 F g^{-1} at a current density of 1 A g^{-1}		95.3% Capacitance retention after 5000 cycles at a high current density of 5 A g^{-1}	2 M KOH aqueous solution	[50]
6	Hollow $ZnCo_2O_4$ microspheres	Solvothermal	78.89 mAh g^{-1} at a current density of 0.2 A g^{-1}		Stability after 2000 cycles	6 M KOH aqueous solution	[51]
7	$ZnCo_2O_4$:activated carbon	Solvothermal	34.7 mAh g^{-1} at a current density of 0.2 A g^{-1}			3 M KOH aqueous solution	
8	$ZnCo_2O_4$ nanomaterial	Hydrothermal	290.5 F g^{-1} at a current density of 0.5 A g^{-1}			2 M KOH aqueous solution	[52]
9	$ZnCo_2O_4$–ethylene glycol symmetric	Hydrothermal	16.7 F g^{-1} at a current density of 0.025 A g^{-1}			2 M KOH aqueous solution	
10	Hexagonal-like shape composed of numerous $ZnCo_2O_4$ NPs	Facile hydrothermal process	1152.19 F g^{-1} at a current density of 5 A g^{-1}		Cycling ability even after 3000 cycles at 50 mV s^{-1} scan rate	2 M KOH aqueous solution	[74]
11	Porous $ZnCo_2O_4$ microspheres	Solvothermal	542.5 F g^{-1} at a current density of 1 A g^{-1} or 217 C g^{-1}	55.3% Capacity retention at 10 A g^{-1}	95.5% Retention of the maximum capacitance (440 F g^{-1}) after 2000 cycles at 2 A g^{-1}	6 M KOH aqueous solution	[75]
12	Mesoporous $ZnCo_2O_4$ nanoflakes grown on nickel foam	Hydrothermal	1220 F g^{-1} at a current density of 2 A g^{-1}		94.2% Capacity retention after 5000 cycles	2 M KOH aqueous solution	[76]
13	Hierarchical coral-like $ZnCo_2O_4$ nanostructures	Facile hydrothermal synthesis	694 F g^{-1} at a current density of 2 A g^{-1}	264 F g^{-1} at 10 A g^{-1}	85% Capacitance retention after 2000 cycles at current density of 10 A g^{-1}	2 M KOH aqueous solution	[77]

Table 1 (continued)

Sr	Properties Electro-active materials	Synthesis route	Specific capacity (C g^{-1}) or specific capacitance (F g^{-1})	Rate property	Cyclic stability	Electrolyte	References
14	$ZnCo_2O_4$ microspheres	Facile ethylene glycol-mediated hydrothermal method	853.6 F g-1 at a current density of 2 A g^{-1}	417.1 F g^{-1} at 10 Ag^{-1}	92.7% capacitance retention after 3000 cycles at a current density of 10 A g^{-1}	2 M KOH aqueous solution	[78]
15	$ZnCo_2O_4$ nanorods on a Ni wire	Facile hydrothermal synthesis	10.9 F g^{-1}		92% Capacitance retention at 2 mA after 3500 charge/discharge cycle	3 M KOH aqueous solution	[79]
16	$ZnCo_2O_4$ rod-like	Solvothermal	302 C g^{-1} at current density of 1 A g^{-1}		95.62% After 3000 cycles at 5 A g^{-1}	6 M KOH aqueous solution	[39]
17	$ZnCo_2O_4$ nanoparticles	Solvothermal	451 F g^{-1}		97.9% After 1500 cycles at 2 A g^{-1}	6 M KOH aqueous solution	[80]
18	Self-assembled hierarchical peony-like $ZnCo_2O_4$	Effective and additive-free	440 F g^{-1} at current density of 1 A g^{-1}		155.6% After 3000 cycles at 2 A g^{-1}	3 M KOH aqueous solution	[81]
19	$ZnCo_2O_4$	Co-precipitation	77 F g^{-1}			6 M KOH aqueous solution	[82]
20	Flower-like $ZnCo_2O_4$ microspheres	Hydrothermal	689.4 F g^{-1} at current density of 1 A g^{-1}	336.6 F g^{-1} at 15 A g^{-1}	97.1% After 1500 cycles at a high current density of 10 A^{-1}	2 M KOH aqueous solution	[83]
21	Mesoporous $ZnCo_2O_4$ microspheres	Solvothermal	953.2 F g^{-1} and 768.5 F g^{-1} at current densities of 4 A g^{-1} and 30 A g^{-1} respectively		97.8% After 3000 cycles	2 M KOH aqueous solution	[84]
22	Hierarchical porous $ZnCo_2O_4$ microspheres	Solvothermal combining with annealing	647.1 F g^{-1} at current densities 1 A g^{-1} and 440.6 F g^{-1} at 10 A g^{-1}, respectively		91.5% After 2000 cycles	2 M KOH aqueous solution	[85]
23	Mesoporous $ZnCo_2O_4$ nanosheet arrays on Ni foam	Hydrothermal	2468, 2382, 2217, 2128, 1904, 1740, 1616 and 1482 F g^{-1} at current densities of 5, 8, 15, 20, 40, 60, 80 and 100 A g^{-1}, respectively		40% Capacity retention when current densities from 5 to 100 A g^{-1} respectively	2 M KOH aqueous solution	[46]
24	$ZnCo_2O_4$ nanocrystals	Sol–gel	575 F g^{-1}		95% Capacity retention after 3000 cycles	1 M NaOH aqueous solution	[86]
25	$ZnCo_2O_4$ nanowire cluster arrays on Ni foam	Hydrothermal	1620 F g^{-1} at current density of 8 A g^{-1}		90% Capacity retention after 6000 cycles	3 M KOH aqueous solution	[87]

Table 1 (continued)

Sr	Properties Electro-active materials	Synthesis route	Specific capacity ($C\ g^{-1}$) or specific capacitance ($F\ g^{-1}$)	Rate property	Cyclic stability	Electrolyte	References
26	Hierarchical $NiCo_2O_4$ nanosheets@hollow microrod arrays	Template-assisted electrode position followed by thermal annealing	678 $F\ g^{-1}$ at current density of 6 $A\ g^{-1}$		96.06% Capacity retention after 1500 cycles	1.0 M KOH aqueous solution	[88]
27	$ZnCo_2O_4$ nanoflowers/NGN/CNT//NGN/CNT	Facile hydrothermal way and subsequent thermal procedure	1802 $F\ g^{-1}$ at current density of 1 $A\ g^{-1}$ or 119 $F\ g^{-1}$ at 0.5 current density $A\ g^{-1}$		Almost 0% capacity retention after 4000 sustaining charge/discharge at 10 $A\ g^{-1}$	2 M KOH aqueous solution or 6 M KOH aqueous solution	[89]
28	$ZnCo_2O_4$ porous nanotubes	Electro-spinning	770 $F\ g^{-1}$ at current density of 10.0 $A\ g^{-1}$		89.5% Retention after 3000 cycles	6 M KOH aqueous solution	[90]
29	$ZnCo_2O_4$ nanowire arrays	Hydrothermal	1625 $F\ g^{-1}$ at current density of 5.0 $A\ g^{-1}$		91.5% retention after 2000 cycles	3 M KOH aqueous solution	[91]
30	Flower-like $ZnCo_2O_4$ microspheres	Hydrothermal	689.4 $F\ g^{-1}$ at current density of 1.0 $A\ g^{-1}$		97.1% Retention after 1500 cycles	2 M KOH aqueous solution	[92]
31	$ZnCo_2O_4$ nanowire arrays	Hydrothermal	1625 $F\ g^{-1}$ at current density of 5.0 $A\ g^{-1}$			3 M KOH aqueous solution	[93]
32	$CoMn_2O_4$ nanowire	Thermal decomposition	2108 $F\ g^{-1}$ at current density of 1 $A\ g^{-1}$ and 1191 $F\ g^{-1}$ at current density of 20 $A\ g^{-1}$				[94]
33	$MnCo_2O_4$ nanowire	Thermal decomposition	1342 $F\ g^{-1}$ at current density of 1 $A\ g^{-1}$ and 988 $F\ g^{-1}$ at current density of 20 $A\ g^{-1}$				
34	$FeCo_2O_4$ nanoflakes	Hydrothermal	2468 $F\ g^{-1}$ at current density of 5.0 $A\ g^{-1}$		94% Retention after 2000 cycles	2 M KOH aqueous solution	[95]
35	Novel three-dimensional $NiCo_2O_4$ hierarchitectures	Solvothermal	647.1 $F\ g^{-1}$ at current density of 1.0 $A\ g^{-1}$		91.5% Retention after 2000 cycle	2 M KOH aqueous solution	[96]
36	Bundles of $ZnCo_2O_4$ nanoparticles	Co-precipitation	159, 138, 117, 88, 65 and 42 $F\ g^{-1}$ for 2, 3, 4, 5, 7.5 and 10 $mA\ cm^{-2}$ current density correspondingly		92% Capacity retention after 2500 cycles	2 M KOH aqueous solution	Present work

protons in the materials [97]. From this impedance analysis, the prepared zinc cobaltite has shown excellent electrochemical capacitive features. Therefore, it can be concluded that the facile synthesis of $ZnCo_2O_4$ more suitable for the application of the supercapacitor.

4 Conclusion

Spinel $ZnCo_2O_4$ nanostructure was successfully synthesized using a facile co-precipitation approach and the final product was investigated in detail. The surface and morphology analysis of the as-prepared electrode showed an aggregated bundle like nanostructures. The optical energy gap was calculated as ~ 3.8 eV. The presence of functional associated with Zn and Co were recorded by FTIR and Raman analysis. XPS analysis confirmed the excited state of Zn and Co in the as-prepared $ZnCo_2O_4$ nanostructure. Finally, the electrochemical investigation of electrode material showed the highest capacitance of 159 F g^{-1} and the long cycle test demonstrated the capacitance retention over 2500 cycles at 5 mA cm^{-2}. This kind of bundle like nanostructure might hold great potential for the next generation of energy storage devices.

Acknowledgements The authors would like to express their gratitude to the Deanship of Scientific Research at King Khalid University, Abha, Saudi Arabia for funding this work through Research Groups Program under Grant No. R.G.P.2/103/41.

Declarations

Conflict of interest The authors declared that there is no conflict of interest.

References

1. B.E. Conway, *Electrochemical Supercapacitors: Scientific Fundamentals and Technological Applications* (Springer, New York, 2013)
2. K.K. Kar, *Handbook of Nanocomposite Supercapacitor Materials II* (Springer, Cham, 2020)
3. S. Ratha, A.K. Samantara, *Supercapacitor: Instrumentation, Measurement and Performance Evaluation Techniques* (Springer, Singapore, 2018)
4. B. Ashok, R.T.K. Raj, K. Nanthagopal, R. Krishnan, R. Subbarao, Lemon peel oil—a novel renewable alternative energy source for diesel engine. Energy Convers. Manag. **139**, 110–121 (2017)
5. H. Nehrir, C. Wang, K. Strunz, H. Aki, R. Ramakumar, J. Bing, Z. Miao, Z. Salameh, A review of hybrid renewable/alternative energy systems for electric power generation: configurations, control and applications. In: *2012 IEEE Power and Energy Society General Meeting*, July 2012 (IEEE, 2012), p. 1.
6. G. Zubi, R. Dufo-López, M. Carvalho, G. Pasaoglu, The lithium-ion battery: state of the art and future perspectives. Renew. Sustain. Energy Rev. **89**, 292–308 (2018)
7. L.H. Tseng, C.H. Hsiao, D.D. Nguyen, P.Y. Hsieh, C.Y. Lee, N.H. Tai, Activated carbon sandwiched manganese dioxide/graphene ternary composites for supercapacitor electrodes. Electrochim. Acta **266**, 284–292 (2018)
8. H. Wang, L. Ma, M. Gan, T. Zhou, Design and fabrication of macroporous polyaniline nanorods@graphene-like MoS_2 nanocomposite with high electrochemical performance for supercapacitors. J. Alloy Compd. **699**, 176–182 (2017)
9. Y. Wang, Y. Song, Y. Xia, Electrochemical capacitors: mechanism, materials, systems, characterization and applications. Chem. Soc. Rev. **45**, 5925 (2016)
10. J. Dong, Z. Hu, Z. Jian, D. Yuanyuan, Y. Hongxun, Y. Aihua, 2016 Facile synthesis of a metal–organic framework-derived Mn_2O_3 nanowire coated three-dimensional graphene network for high-performance free-standing supercapacitor electrodes. J. Mater. Chem. A **4**, 8283–8290 (2016)
11. P. Periasamy, T. Krishnakumar, V.P. Devarajan, M. Sandhiya, M. Sathish, M. Chavali, Investigation of electrochemical supercapacitor performance of WO_3–CdS nanocomposites in 1 M H_2SO_4 electrolyte prepared by microwave-assisted method. Mater. Lett. **274**, 127998 (2020)
12. P. Periasamy, T. Krishnakumar, M. Sathish, M. Chavali, P.F. Siril, V.P. Devarajan, 2-D nanostructures of advanced hybridized for high performance WO_3 nanocomposites of supercapacitor application. In: *Nanostructured Materials and Their Applications* (Springer, Singapore, 2020), p. 1.
13. A. Eftekhari, L. Li, Y. Yang, Polyaniline supercapacitors. J. Power Sources **347**, 86–107 (2017)
14. X. He, H. Ma, J. Wang, Y. Xie, N. Xiao, J. Qiu, Porous carbon nanosheets from coal tar for high-performance supercapacitors. J. Power Sources **357**, 41–46 (2017)
15. L. Wang, R. Wang, H. Zhao, L. Liu, D. Jia, High rate performance porous carbon prepared from coal for supercapacitors. Mater. Lett. **149**, 85–88 (2015)
16. Z. Wang, H. Qiang, C. Zhang, Z. Zhu, M. Chen, C. Chen, D. Zhang, Facile fabrication of hollow polyaniline spheres and its application in supercapacitor. J. Polym. Res. **25**, 129 (2018)
17. N. Padmanatha, S. Selladurai, Shape controlled synthesis of CeO_2 nanostructures for high performance supercapacitor electrodes. RSC Adv. **4**, 6527–6534 (2014)
18. X. Li, J. Shao, J. Li, L. Zhang, Q. Qu, H. Zheng, Ordered mesoporous MoO_2 as a high-performance anode material for aqueous supercapacitors. J. Power Sources **37**, 80–83 (2013)
19. C.V. Reddy, C. Byon, B. Narendra, B. Dudem, J. Shim, S.J. Moon, S.P. Vattikuti, Effect of calcination temperature on cobalt substituted cadmium ferrite nanoparticles. J. Mater. Sci. Mater. Electron. **26**(7), 5078–5084 (2015)
20. T.V.M. Sreekanth, R. Ramaraghavulu, S.P. Vattikuti, J. Shim, K. Yoo, Microwave synthesis: $ZnCo_2O_4$ NPs as an efficient electrocatalyst in the methanol oxidation reaction. Mater. Lett. **253**, 450–453 (2019)
21. P.C. Nagajyothi, K.C. Devarayapalli, J. Shim, S.P. Vattikuti, Highly efficient white-LED-light-driven photocatalytic hydrogen production using highly crystalline $ZnFe_2O_4$/MoS_2 nanocomposites. Int. J. Hydrog. Energy **45**(57), 32756–32769 (2020)
22. B. Poornaprakash, U. Chalapathi, S.V. Prabhakar Vttikuti, P. Reddy, S.H. Park, Pristine and Sm-doped ZnS quantum dots: structural, optical, luminescence, magnetic, and photocatalytic properties. Chalcogenide Lett. **16**(2), 49–55 (2019)
23. S.P. Vattikuti, A.K.R. Police, J. Shim, C. Byon, Sacrificial-template-free synthesis of core–shell C@ Bi_2S_3 heterostructures for

efficient supercapacitor and H_2 production applications. Sci. Rep. **8**(1), 1–16 (2018)
24. S.P. Vattikuti, B.P. Reddy, C. Byon, J. Shim, Carbon/CuO nanosphere-anchored g-C_3N_4 nanosheets as ternary electrode material for supercapacitors. J. Solid State Chem. **262**, 106–111 (2018)
25. A.K.R. Police, S.P. Vattikuti, Y.J. Baik, B. Chan, Eco-friendly, hydrogen fluoride-free, morphology-oriented synthesis of TiO_2 with exposed (001) facets. Ceram. Int. **45**(2), 2178–2184 (2019)
26. F. Razi, S. Zinatloo-Ajabshir, M. Salavati-Niasari, Preparation and characterization of HgI_2 nanostructures via a new facile route. Mater. Lett. **193**, 9–12 (2017)
27. S. Zinatloo-Ajabshir, S. Mortazavi-Derazkola, M. Salavati-Niasari, Nd_2O_3 nanostructures: simple synthesis, characterization and its photocatalytic degradation of methylene blue. J. Mol. Liq. **234**, 430–436 (2017)
28. S. Zinatloo-Ajabshir, S. Mortazavi-Derazkola, M. Salavati-Niasari, Preparation, characterization and photocatalytic degradation of methyl violet pollutant of holmium oxide nanostructures prepared through a facile precipitation method. J. Mol. Liq. **231**, 306–313 (2017)
29. S. Zinatloo-Ajabshir, M. Salavati-Niasari, Zirconia nanostructures: novel facile surfactant-free preparation and characterization. Int. J. Appl. Ceram. Technol. **13**(1), 108–115 (2016)
30. S. Zinatloo-Ajabshir, M. Salavati-Niasari, Preparation and characterization of nanocrystalline praseodymium oxide via a simple precipitation approach. J. Mater. Sci. Mater. Electron. **26**(8), 5812–5821 (2015)
31. S. Zinatloo-Ajabshir, M. Baladi, M. Salavati-Niasari, Enhanced visible-light-driven photocatalytic performance for degradation of organic contaminants using $PbWO_4$ nanostructure fabricated by a new, simple and green sonochemical approach. Ultrason. Sonochem. **72**, 105420 (2021)
32. M. Mousavi-Kamazani, S. Zinatloo-Ajabshir, M. Ghodrati, One-step sonochemical synthesis of $Zn(OH)_2/ZnV_3O_8$ nanostructures as a potent material in electrochemical hydrogen storage. J. Mater. Sci. Mater. Electron. **31**(20), 17332–17338 (2020)
33. S. Zinatloo-Ajabshir, N. Ghasemian, M. Mousavi-Kamazani, M. Salavati-Niasari, Effect of zirconia on improving NO_x reduction efficiency of $Nd_2Zr_2O_7$ nanostructure fabricated by a new, facile and green sonochemical approach. Ultrason. Sonochem. **71**, 105376 (2021)
34. S. Zinatloo-Ajabshir, M. Mousavi-Kamazani, Effect of copper on improving the electrochemical storage of hydrogen in CeO_2 nanostructure fabricated by a simple and surfactant-free sonochemical pathway. Ceram. Int. **46**(17), 26548–26556 (2020)
35. S. Zinatloo-Ajabshir, M.S. Morassaei, O. Amiri, M. Salavati-Niasari, Green synthesis of dysprosium stannate nanoparticles using *Ficus carica* extract as photocatalyst for the degradation of organic pollutants under visible irradiation. Ceram. Int. **46**(5), 6095–6107 (2020)
36. S. Zinatloo-Ajabshir, S.A. Heidari-Asil, M. Salavati-Niasari, Recyclable magnetic $ZnCo_2O_4$-based ceramic nanostructure materials fabricated by simple sonochemical route for effective sunlight-driven photocatalytic degradation of organic pollution. Ceram. Int. **47**(7), 8959–8972 (2021)
37. A. Ray, A. Roy, M. Ghosh, J.A. Ramos-Ramón, S. Saha, U. Pal, S.K. Bhattacharya, S. Das, Study on charge storage mechanism in working electrodes fabricated by sol–gel derived spinel $NiMn_2O_4$ nanoparticles for supercapacitor application. Appl. Surf. Sci. **463**, 513–525 (2019)
38. X. Zhu, Z. Wei, W. Zhao, X.D. Zhang, X.J. Wu, J.L. Jiang, Preparation and characterization of $Zn_{1-x}Ni_xFe_2O_4$ nanoparticles with spinel structure synthesized by hydrothermal method. Curr. Nanosci. **14**(6), 474–480 (2018)
39. T. Huang, C. Zhao, R. Zheng, Y. Zhang, Z. Hu, Facilely synthesized porous $ZnCo_2O_4$ rodlike nanostructure for high-rate supercapacitors. Ionics **21**, 3109–3115 (2015)
40. S. Vijayanand, P.A. Joy, H.S. Potdar, D. Patil, P. Patil, Nanostructured spinel $ZnCo_2O_4$ for the detection of LPG. Sens. Actuators B **152**, 121–129 (2011)
41. B. Liu, X. Wang, B. Liu, Q. Wang, D. Tan, W. Song, X. Hou, D. Chen, G. Shen, Advanced rechargeable lithium-ion batteries based on bendable $ZnCo_2O_4$-urchins-on-carbon-fibers electrodes. Nano Res. **6**, 525–534 (2013)
42. B. Liu, J. Zhang, X. Wang, G. Chen, D. Chen, C. Zhou, G. Shen, Hierarchical three-dimensional $ZnCo_2O_4$ nanowire arrays/carbon cloth anodes for a novel class of high-performance flexible lithium-ion batteries. Nano Lett. **12**, 3005–3011 (2012)
43. W. Shubo, P. Jun, T. Yao, C. Yuanyuan, G. Yan, W. Zhenghua, $ZnCo_2O_4$ nanowire arrays grown on nickel foam for high-performance pseudocapacitors. J. Mater. Chem. A **2**, 5434–5440 (2014)
44. L. Bin, L. Boyang, W. Qiufan, W. Xianfu, X. Qingyi, C. Di, S. Guozhen, New energy storage option: toward $ZnCo_2O_4$ nanorods/nickel foam architectures for high-performance supercapacitors. ACS Appl. Mater. Interfaces **5**, 10011–10017 (2013)
45. G. Zhou, J. Zhu, Y. Chen, L. Mei, X. Duan, G. Zhang, L. Chen, T. Wang, B. Lu, Simple method for the preparation of highly porous $ZnCo_2O_4$ nanotubes with enhanced electrochemical property for supercapacitor. Electrochim. Acta **123**, 450–455 (2014)
46. F. Bao, X. Wang, X. Zhao, Y. Wang, Y. Ji, H. Zhang, X. Liu, Controlled growth of mesoporous $ZnCo_2O_4$ nanosheet arrays on Ni foam as high-rate electrodes for supercapacitors. RSC Adv. **4**, 2393–2397 (2014)
47. L. Xu, Y. Zhao, J. Lian, Y. Xu, J. Bao, J. Qiu, L. Xu, H. Xu, M. Hua, H. Li, Morphology controlled preparation of $ZnCo_2O_4$ nanostructures for asymmetric supercapacitor with ultrahigh energy density. Energy **123**, 296–304 (2017)
48. B. Liu, B. Liu, Q. Wang, X. Wang, Q. Xiang, D. Chen, G. Shen, New energy storage option: toward $ZnCo_2O_4$ nanorods/nickel foam architectures for high-performance supercapacitors. ACS Appl. Mater. Interfaces **5**(20), 10011–10017 (2013)
49. Y.A. Kumar, K.D. Kumar, H.J. Kim, Reagents assisted $ZnCo_2O_4$ nanomaterial for supercapacitor application. Electrochim. Acta **330**, 135261 (2020)
50. V. Venkatachalam, A. Alsalme, A. Alswieleh, R. Jayavel, Double hydroxide mediated synthesis of nanostructured $ZnCo_2O_4$ as high performance electrode material for supercapacitor applications. Chem. Eng. J. **321**, 474–483 (2017)
51. Y. Shang, T. Xie, C. Ma, L. Su, Y. Gai, J. Liu, L. Gong, Synthesis of hollow $ZnCo_2O_4$ microspheres with enhanced electrochemical performance for asymmetric supercapacitor. Electrochim. Acta **286**, 103–113 (2018)
52. A.J.C. Mary, A.C. Bose, Surfactant assisted $ZnCo_2O_4$ nanomaterial for supercapacitor application. Appl. Surf. Sci. **449**, 105–112 (2018)
53. M. Masjedi-Arani, M. Salavati-Niasari, Novel synthesis of Zn_2GeO_4/graphene nanocomposite for enhanced electrochemical hydrogen storage performance. Int. J. Hydrog. Energy **42**, 17184–17191 (2017)
54. A. Salehabadi, M. Salavati-Niasari, M. Ghiyasiyan-Arani, Self-assembly of hydrogen storage materials based multi-walled carbon nanotubes (MWCNTs) and $Dy_3Fe_5O_{12}$ (DFO) nanoparticles. J. Alloys Compd. **745**, 789–797 (2018)
55. S. Mortazavi-Derazkola, M. Salavati-Niasari, O. Amiri, A. Abbasi, Fabrication and characterization of $Fe_3O_4@SiO_2@TiO_2@$ Ho nanostructures as a novel and highly efficient photocatalyst for degradation of organic pollution. J. Energy Chem. **26**, 17–23 (2017)

56. S. Zinatloo-Ajabshir, M. Salavati-Niasari, Z. Zinatloo-Ajabshir, $Nd_2Zr_2O_7$–Nd_2O_3 nanocomposites: new facile synthesis, characterization and investigation of photocatalytic behaviour. Mater. Lett. **180**, 27–30 (2016)
57. F. Beshkar, H. Khojasteh, M. Salavati-Niasari, Recyclable magnetic superhydrophobic straw soot sponge for highly efficient oil/water separation. J. Colloid Interface Sci. **497**, 57–65 (2017)
58. F. Ansari, A. Sobhani, M. Salavati-Niasari, Green synthesis of magnetic chitosan nanocomposites by a new sol–gel autocombustion method. J. Magn. Magn. Mater. **410**, 27–33 (2016)
59. F. Ansari, A. Sobhani, M. Salavati-Niasari, Simple sol–gel synthesis and characterization of new $CoTiO_3$/$CoFe_2O_4$ nanocomposite by using liquid glucose, maltose and starch as fuel, capping and reducing agents. J. Colloid Interface Sci. **514**, 723–732 (2018)
60. S. Ahmadian-Fard-Fini, M. Salavati-Niasari, D. Ghanbari, Hydrothermal green synthesis of magnetic Fe3O4–carbon dots by lemon and grape fruit extracts and as a photoluminescence sensor for detecting of *E. coli* bacteria. Spectrochim. Acta A **203**, 481–493 (2018)
61. F. Tavakoli, M. Salavati-Niasari, A. Badiei, F. Mohandes, Green synthesis and characterization of graphene nanosheets. Mater. Res. Bull. **63**, 51–57 (2015)
62. M. Salavati-Niasari, Z. Fereshteh, F. Davar, Synthesis of oleylamine capped copper nanocrystals via thermal reduction of a new precursor. Polyhedron **28**, 126–130 (2009)
63. Y. Einaga, Electrochemical application of diamond electrodes, in *Comprehensive Hard Materials*. ed. by V.K. Sarin (Elsevier, Oxford, 2014), pp. 493–512
64. M. Maddahfar, M. Ramezani, M. Sadeghi, A. Sobhani-Nasab, $NiAl_2O_4$ nanoparticles: synthesis and characterization through modify sol–gel method and its photocatalyst application. J. Mater. Sci. Mater. Electron. **26**, 7745–7750 (2015)
65. L. Ren, P. Wang, Y. Han, C. Hu, B. Wei, Synthesis of $CoC_2O_4{\cdot}2H_2O$ nanorods and their thermal decomposition to Co_3O_4 nanoparticles. Chem. Phys. Lett. **476**, 78–83 (2009)
66. X. Wei, D. Chen, W. Tang, Preparation and characterization of the spinel oxide $ZnCo_2O_4$ obtained by sol–gel method. Mater. Chem. Phys. **103**, 54 (2007)
67. B. Hadžić, N. Romčević, M. Romčević, I. Kuryliszyn-Kudelska, W.D. Dobrowolski, U. Narkiewicz, D. Sibera Hemijska, Raman study of surface optical phonons in ZnO (Co) nanoparticles prepared by hydrothermal method. Industrija **67**(2013), 695–771 (2013)
68. N. Padmanathan, H. Shao, D. McNulty, C. ODwyer, K.M. Razeeb, Hierarchical NiO–In_2O_3 microflower (3D)/nanorod (1D) hetero-architecture as a supercapattery electrode with excellent cyclic stability. J. Mater. Chem. A **4**, 4820–4830 (2016)
69. R. Monsef, M. Ghiyasiyan-Arani, M. Salavati-Niasari, Utilizing of neodymium vanadate nanoparticles as an efficient catalyst to boost the photocatalytic water purification. J. Environ. Manag. **230**, 266–281 (2019)
70. R. Monsef, M. Ghiyasiyan-Arani, O. Amiri, M. Salavati-Niasari, Sonochemical synthesis, characterization and application of $PrVO_4$ nanostructures as an effective photocatalyst for discoloration of organic dye contaminants in wastewater. Ultrason. Sonochem. **61**, 104822 (2020)
71. C.R. Mariappan, R. Kumar, G. Vijaya Prakash, Functional properties of $ZnCo_2O_4$ nano-particles obtained by thermal decomposition of a solution of binary metal nitrates. RSC Adv. **5**, 26843–26849 (2015)
72. N. Padmanathan, S. Selladurai, Mesoporous $MnCo_2O_4$ spinel oxide nanostructure synthesized by solvothermal technique for supercapacitor. Ionics **20**(2014), 479–487 (2014)
73. K. Xie, X. Qin, X. Wang, Y. Wang, H. Tao, Q. Wu, L. Yang, Z. Hu, Carbon nanocages as supercapacitor electrode materials. Adv. Mater. **24**, 347–352 (2012)
74. G.M. Tomboc, H.S. Jadhav, H. Kim, PVP assisted morphology-controlled synthesis of hierarchical mesoporous $ZnCo_2O_4$ nanoparticles for high-performance pseudocapacitor. Chem. Eng. J. **308**, 202–213 (2017)
75. Y. Gai, Y. Shang, L. Gong, L. Su, L. Hao, F. Dong, A self-template synthesis of porous $ZnCo_2O_4$ microspheres for high-performance quasi-solid-state asymmetric supercapacitors. RSC Adv. **7**, 1038–1044 (2017)
76. J. Cheng, Y. Lu, K. Qiu, H. Yan, X. Hou, J. Xu, L. Han, X. Liu, J.-K. Kim, Y. Luo, Mesoporous $ZnCo_2O_4$ nanoflakes grown on nickel foam as electrodes for high performance supercapacitors. Phys. Chem. Chem. Phys. **17**, 17016–17022 (2015)
77. J.A. Rajesh, B.-K. Min, J.-H. Kim, S.-H. Kang, H. Kim, K.-S. Ahn, Facile hydrothermal synthesis and electrochemical supercapacitor performance of hierarchical coral-like $ZnCo_2O_4$ nanowires. J. Electroanal. Chem. **785**, 48–57 (2017)
78. J.A. Rajesh, B.-K. Min, J.-H. Kim, S.-H. Kang, H. Kim, K.-S. Ahn, Cubic spinel AB_2O_4 type porous $ZnCo_2O_4$ microspheres: facile hydrothermal synthesis and their electrochemical performances in pseudocapacitor. J. Electrochem. Soc. **163**, A2418–A2427 (2016)
79. H. Wu, Z. Lou, H. Yang, G. Shen, A flexible spiral-type supercapacitor based on $ZnCo_2O_4$ nanorod electrodes. Nanoscale **7**, 1921–1926 (2015)
80. S. Chen, M. Xue, Y. Li, L. Zhu, D. Zhang, Q. Fang, S. Qiu, Porous $ZnCo_2O_4$ nanoparticles derived from a new mixed-metal organic framework for supercapacitors. Inorg. Chem. Front. **2**, 177–183 (2015)
81. Y. Shang, T. Xie, Y. Gai, L. Su, L. Gong, H. Lv, F. Dong, Self-assembled hierarchical peony-like $ZnCo_2O_4$ for high-performance asymmetric supercapacitors. Electrochim. Acta **253**, 281–290 (2017)
82. K. Karthikeyan, D. Kalpana, N.G. Renganathan, Synthesis and characterization of $ZnCo_2O_4$ nanomaterial for symmetric supercapacitor applications. Ionics **15**, 107–110 (2009)
83. W. Fu, X. Li, C. Zhao, Y. Liu, P. Zhang, J. Zhou, X. Pan, E. Xie, Facile hydrothermal synthesis of flower like $ZnCo_2O_4$ microspheres as binder-free electrodes for supercapacitors. Mater. Lett. **149**, 1–4 (2015)
84. Q. Wang, J. Du, Y. Zhu, J. Yang, J. Chen, C. Wang, L. Li, L. Jiao, Facile fabrication and supercapacitive properties of mesoporous zinc cobaltite microspheres. J. Power Sources **284**, 138–145 (2015)
85. Q. Wang, L. Zhu, L. Sun, Y. Liu, L. Jiao, Facile synthesis of hierarchical porous $ZnCo_2O_4$ microspheres for high-performance supercapacitors. J. Mater. Chem. **3**, 982–985 (2015)
86. M. Davis, C. Gumeci, B. Black, C. Korzeniewski, L.H. Weeks, Tailoring cobalt doped zinc oxide nanocrystals with high capacitance activity: factors affecting structure and surface morphology. RSC Adv. **2**, 2061 (2012)
87. B. Guan, D. Guo, L. Hu, G. Zhang, T. Fu, W. Ren, J. Li, Q. Li, Facile synthesis of $ZnCo_2O_4$ nanowire cluster arrays on Ni foam for high-performance asymmetric supercapacitors. J. Mater. Chem. A **2**, 16116–16123 (2014)
88. X. Lu, D. Wu, R. Li, Q. Li, S. Ye, Y. Tong, G. Li, Hierarchical $NiCo_2O_4$ nanosheets@hollow microrod arrays for high-performance asymmetric supercapacitors. J. Mater. Chem. A **2**, 4706–4713 (2014)
89. W. Bai, H. Tong, Z. Gao, S. Yue, S. Xing, S. Dong, L. Shen, J. He, X. Zhang, Y. Liang, Preparation of $ZnCo_2O_4$ nanoflowers on a 3D carbon nanotube/nitrogen-doped graphene film and its

electrochemical capacitance. J. Mater. Chem. A **3**, 21891–21898 (2015)
90. B. Liu, J. Zhang, X. Wang, G. Chen, D. Chen, C. Zhou, G. Shen, Hierarchical three-dimensional $ZnCo_2O_4$ nanowire arrays/carbon cloth anodes for a novel class of high performance flexible lithium-ion batteries. Nano Lett. **12**, 3005 (2012)
91. C. Wu, J. Cai, Q. Zhang, X. Zhou, Y. Zhu, P.K. Shen, K. Zhang, Hierarchical mesoporous zinc–nickel–cobalt ternary oxide nanowire arrays on nickel foam as high-performance electrodes for supercapacitors. ACS Appl. Mater. Interfaces **7**, 26512–26521 (2015)
92. D. Zhang, Y. Zhang, X. Li, Y. Luo, H. Huang, J. Wang, P.K. Chu, Self-assembly of mesoporous $ZnCo_2O_4$ nanomaterials: density functional theory calculation and flexible all-solid-state energy storage. J. Mater. Chem. A **4**, 568–577 (2016)
93. S. Wang, J. Pu, Y. Tong, Y. Cheng, Y. Gao, Z. Wang, $ZnCo_2O_4$ nanowire arrays grown on nickel foam for high-performance pseudocapacitors. J. Mater. Chem. A **2**, 5434 (2014)
94. Y. Xu, X. Wang, C. An, Y. Wang, L. Jiao, H. Yuan, Facile synthesis route of porous $MnCo_2O_4$ and $CoMn_2O_4$ nanowires and their excellent electrochemical properties in supercapacitors. J. Mater. Chem. A **2**, 16480–16488 (2014)
95. S.G. Mohamed, C.-J. Chen, C.K. Chen, S.-F. Hu, R.-S. Liu, High-performance lithium ion battery and symmetric supercapacitors based on $FeCo_2O_4$ nanoflakes electrodes. ACS Appl. Mater. Interfaces **6**, 22701–22708 (2014)
96. C. An, Y. Wang, Y. Huang, Y. Xu, C. Xu, L. Jiao, H. Yuan, Novel three-dimensional $NiCo_2O_4$ hierarchitectures: solvothermal synthesis and electrochemical properties. CrystEngComm **16**, 385–392 (2014)
97. Z. Niu, P. Luan, Q. Shao, H. Dong, L. Li, J. Chen, D. Zhao, L. Cai, W. Zhou, X. Chen, A “skeleton/skin” strategy for preparing ultrathin free-standing single-walled carbon nanotube/polyaniline films for high performance supercapacitor electrodes. Energy Environ. Sci. **5**, 8726–8733 (2012)